



# Suggesting a new modification of the Cole–Cole model for the purposes of explaining and describing the optical dielectric relaxation phenomena

Hosam M. Gomaa<sup>1</sup> · H. A. Saudi<sup>2</sup> · Saeid M. Elkatlaw<sup>3</sup> · H. Y. Zahran<sup>4</sup> · I. S. Yahia<sup>4</sup>

Received: 22 June 2023 / Accepted: 21 August 2023 / Published online: 4 September 2023  
© The Author(s), under exclusive licence to Springer-Verlag GmbH, DE part of Springer Nature 2023

## Abstract

Cole–Cole model for electric–dielectric relaxation has been developed to be applicable in the case of optical dielectric relaxation. Such achievement, in addition to Tauc's relationship, should help in exacting the extracted optical parameters of an optical medium for the purposes of optoelectronic applications. One sample of barium lead sodium borate glass has been prepared using the traditional techniques and methods. The amorphous nature prepared of the sample has been characterized using both the X-ray diffraction XRD technique and Fourier transform infrared FTIR spectral analysis. XRD pattern revealed only two broad humps, while FTIR spectrum revealed the existence of three basic structural units  $\text{BO}_3$ ,  $\text{BO}_4$ , and  $\text{PbO}_4$ . While UV–Vis optical measurements showed the prepared sample is of low optical transmittance (high absorption rate per meter). The optical analysis showed that both the surface, SELF, and volume, VELF, energy loss functions decreased as the photon's frequency increased. The SELF values are found to be lesser than the VELF values, which means that the prepared sample has a high absorption rate and a low reflection rate at all UV–Vis regions. Finally, the Cole–Cole approximation has been modified successively, by the first author Hosam M Gomaa, to simulate and describe the optical dielectric relaxation for the prepared glass, where the resulting parameters helped in determining the number of relaxation processes that contributed to the optical spectrum. The new approximation helped in determining the hidden absorption peaks in the UV region. The resulted Cole–Cole parameter showed small values (less than unity), confirming the amorphous nature of the prepared sample.

**Keywords** Borate oxide glasses · UV–Vis spectral analysis · Modified Cole–Cole · Optical dielectric relaxation

## 1 Introduction

Borate-based oxide glasses have been catching interest in both research and industrial sectors, for their notable and unique properties [1–3]. These glasses possess exceptional peculiarities that can be controlled to fit many scientific and

technological applications, such as optical fibers, laser active media, semiconductors, microelectronics, and scintillation detectors [4–6]. Addition of impurities like bismuth oxide led to improving overall properties of the borate glass by changing the internal structural arrangement of borosilicate glasses [7–10].

UV–visible spectral analysis is very useful in the characterization of the glass electronic structure as well as the glass network homogeneity. Where it is well known that the optical properties are closely linked with the atomic and electronic band structures of the material [11]. Studies of dielectric properties showed improved characteristics of different compositions of BOGs for electronic applications [12–14]. On the other hand, interaction of light with an optical solid affects its electronic structure by means of material polarization and subsequently creates up what is called optical dielectric relaxation. In general, the dielectric relaxation is a complex quantity depending on the type of physical defects related to the dipoles within the sample [15]. The optical

✉ Hosam M. Gomaa  
h\_goumaa@yahoo.com

<sup>1</sup> Pharaohs-Higher Institute for Computer, Information Systems and Management, Giza, Egypt

<sup>2</sup> Department of Physics, Faculty of Science, Al-Azhar University (Girls' Branch), Cairo, Egypt

<sup>3</sup> Department of Physics, Faculty of Science, Damanhour University, Damanhour 22111, Egypt

<sup>4</sup> Laboratory of Nano-Smart Materials for Science and Technology (LNSMST), Department of Physics, Faculty of Science, King Khalid University, P. O. Box 9004, Abha, Saudi Arabia

dielectric relaxation process is a phenomenon that occurs in optical materials. It is the process by which the polarization of a material relaxes back to its equilibrium state after being perturbed by an external electric field. This process is characterized by the dielectric relaxation time which is the time it takes for the polarization to relax back to its equilibrium state. The well-known Cole–Cole empirical model [16] has been used for the studies of different dielectric parameters and the relaxation time of dielectric materials.

This paper is concerned with developing the Cole–Cole model for dielectric relaxation to be useful in the extraction of the optical parameters of an optical medium based on its recorded UV–Vis charts. In more details, the current study aims to extend this Cole–Cole approximation to describe the optical dielectric relaxation processes due to light interaction within an optical oxide-glass sample. This paper is not a competitive study, it does not focus on either the preparation or characterization of glass, and it just aims to develop the Cole–Cole equation for electrical dielectric relaxation to be suitable in describing optical dielectric relaxation. The used glass system has been used as an example of the optical material to perform the study and extract the results. It is expected that the current study will result in the foundation of a new method to determine the optical band gap which is an essential factor in the description of semiconductors and insulators, as well as reflects the fine structural changes, because it reveals details about the electrical structure of materials and their optical characteristics, so the determination of the optical band gap is crucial.

## 2 Experimental methodology

Sigma-Aldrich's chemicals of purity do not less than 98% have been used to prepare one glass sample of composition [50 mol% B<sub>2</sub>O<sub>3</sub>–25 mol% Na<sub>2</sub>O–12.5 mol% BaO–12.5 mol% PbO], where all used oxides were weighted using an electrical balance and then melted in a porcelain crucible at 1150 °C in an electrically heated furnace for 90 min., before quenched by pouring at room-temperature air in between two copper plates. The resulted solids were examined using Philips analytical X-ray diffraction. X-ray unit kept constant at 40 kV with a current of 30 mA. FTIR measured using an infrared spectrometer (type JASCO FT/IR-4100), while the optical absorption spectra were examined using a spectrophotometer (type JASCO, V-570).

## 3 Results and discussion

### 3.1 Structural characterization: XRD & FTIR:

Figure 1 shows the X-ray diffraction (XRD) pattern of the prepared sample, where only two broad humps can

be observed and no evidence of sharp peaks, which confirms the amorphous nature of this sample. Accordingly, it can be stated that the prepared sample can be considered as high-quality oxide-glass optical material. The internal structure of this sample has been verified using Fourier transform infrared spectra (FTIR), as shown in Fig. 2, which displays the FTIR absorption spectrum of the prepared sample versus the photon wavelength (nm) instead of the wavenumber (cm<sup>-1</sup>). Where the using of the wavelength rather than the wavenumber is acceptable, and in the present work, it resulted in a much clearer IR spectral chart. Figure 2 reveals six main absorption bands due to six different functional groups and vibrational bonds, and these absorption bands are assigned to their originators and are tabulated in Table 1.

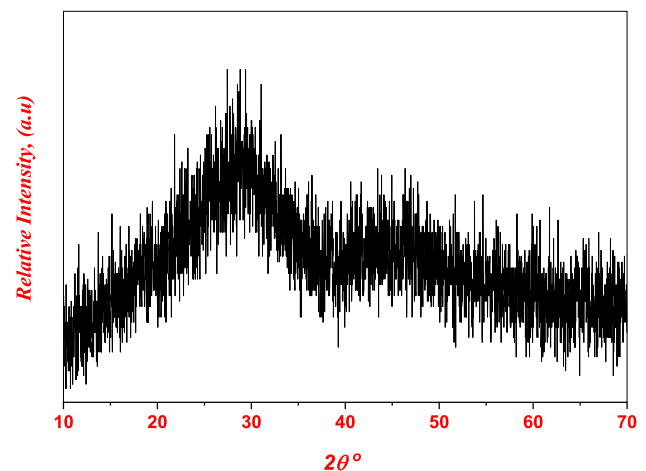


Fig. 1 Powder XRD patterns for the glassy sample

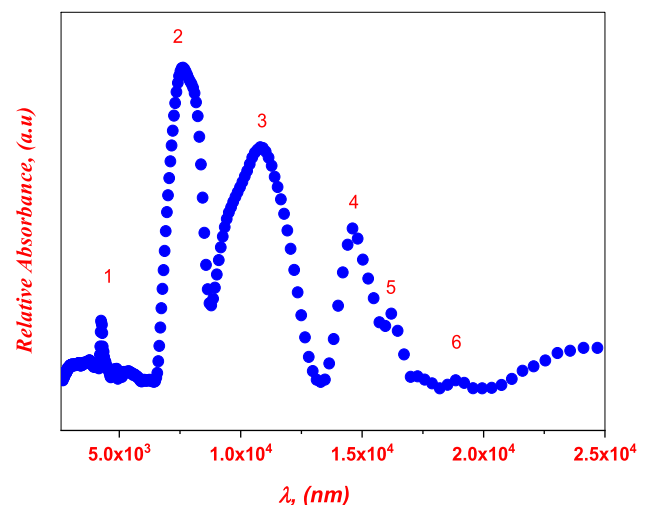
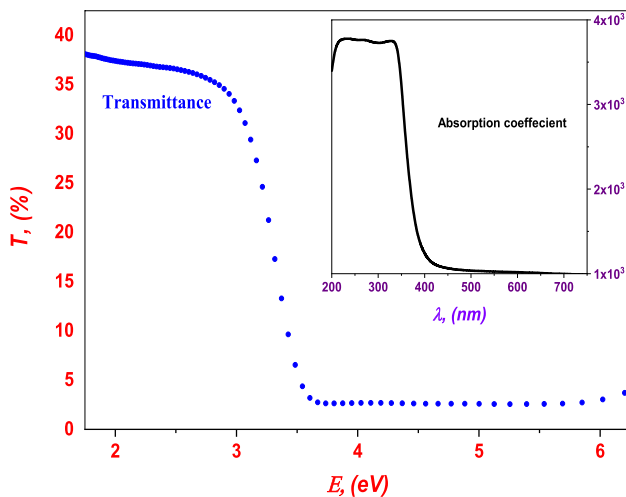


Fig. 2 Normalized FTIR spectrum of the studied sample

**Table 1** FTIR absorption detectable peaks

Peak center	$\lambda$ , nm	$\lambda$ , cm	$\nu$ , 1/cm	Assignments	Refs
1	4274	0.0004	2340	OH- groups	[17]
2	7681	0.0008	1302	BO <sub>3</sub> glass former groups-stretching vibrations	[18]
3	10,913	0.0011	916	BO <sub>4</sub> glass former groups-stretching vibrations	[19]
4	14,663	0.0015	682	O <sub>2</sub> B–O–BO <sub>3</sub> linkages/bonds	[20]
5	16,238	0.0016	616	PbO <sub>4</sub> glass former groups	[21]
6	18,866	0.0019	530	Ba–O-bond specific vibration	[22]

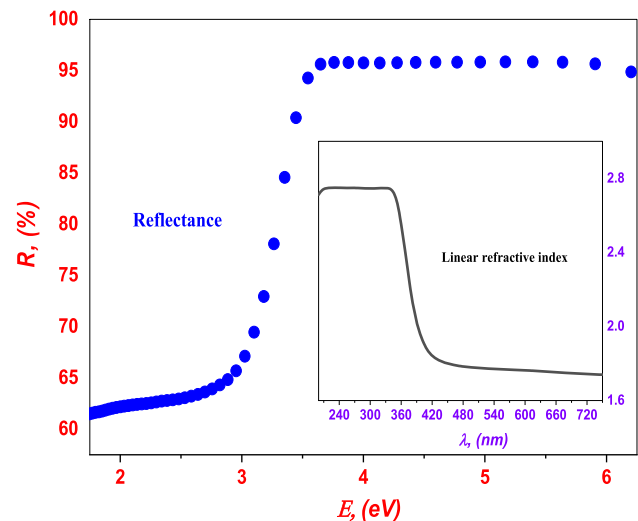
**Fig. 3** Optical transmittance and the absorption coefficient (inset) for the studied sample

### 3.2 Optical characterization

The optical characterization using UV–Vis spectral analysis is a basic technique for a good understanding of the electronic transitions in glasses, and it defines the type of structural network formers as well as the imperfections in the glass structure. Accordingly, the UV–Vis spectra have been recorded for the studied sample using double beam spectrometer in the range of 190–2500 nm. However, this study is limited to the range of 190–750 nm.

Figure 3 shows the change in the percentage of optical transmittance ( $T\%$ ) and the optical absorption coefficient ( $\alpha$ ), where it shows a low transmittance value (less than 40% of the incident rays), which may be due to the equal concentration of the heavy metal cations,  $\text{Pb}^{2+}$  and  $\text{Ba}^{2+}$ , which are good energy attenuation agents, especially in the high-energy region where the electronic transitions have a high probability. While inset figure shows relatively high values (near  $4000 \text{ m}^{-1}$ ) for the absorption coefficient ( $\alpha$ ) in UV region, which explain the dip in the  $T\%$  value. Where the refractive index was determined based on the values of the optical reflectance ( $R$ ) and the absorption coefficient ( $\alpha$ ), Eqs. 1, 2 [23–25].

Figure 4 exhibits the change in measured reflectance ( $R$ ) and the linear refractive index ( $n$ ). The observable high value

**Fig. 4** Optical reflectance and linear refractive index (inset) for the studied sample

of reflectance (60–96%) at almost all energy regions may indicate a high optical energy loss

$$n = \left( \frac{1 + 0.25R}{1 - 0.25R} \right) + \sqrt{\frac{R\%}{(1 - 0.25R)^2} - \left( \frac{\alpha\lambda}{4\pi} \right)^2} \quad (1)$$

(where  $n$  is the linear refractive index,  $R$  is the optical reflectance,  $\alpha$  is the optical absorption coefficient, and  $\lambda$  is the wavelength of the incident photons)

$$\alpha = \frac{2.303}{t} (1 - T - R) \quad (2)$$

(where  $\alpha$  is the optical absorption coefficient,  $T$  is the optical transmittance,  $R$  is the optical reflectance, and  $t$  is the sample thickness).

The loss of energy can be expressed by the optical dielectric relaxation  $\epsilon^*$  parameter, Eq. 3 [20], which consists of a real ( $\epsilon'$  dielectric constant) and an imaginary ( $\epsilon''$  dielectric loss) components. For unfree damper, the real component ( $\epsilon'$ ) characterizes the damping of the light propagation through the medium. While the imaginary component is considered a damping factor that describes the amount of energy lost/absorbed within the medium [26, 27]. Where

both components have been calculated for all studied samples using Eq. 4 for ( $\epsilon'$  dielectric constant) and Eq. 5 for ( $\epsilon''$  dielectric loss) [27]

$$\epsilon^* = \epsilon' + j\epsilon'' \tag{3}$$

(where  $\epsilon^*$  is the complex dielectric function,  $\epsilon'$  is the real dielectric constant, and  $\epsilon''$  is the dielectric loss)

$$\epsilon' = n^2 - \left(\frac{\alpha\lambda}{4\pi}\right)^2 \tag{4}$$

(where  $\epsilon'$  is the real dielectric constant,  $n$  is the linear refractive index,  $\alpha$  is the optical absorption coefficient, and  $\lambda$  is the wavelength of the incident photons)

$$\epsilon'' = 2n\frac{\alpha\lambda}{4\pi} \tag{5}$$

(where  $\epsilon''$  is the real dielectric loss,  $n$  is the linear refractive index,  $\alpha$  is the optical absorption coefficient, and  $\lambda$  is the wavelength of the incident photons).

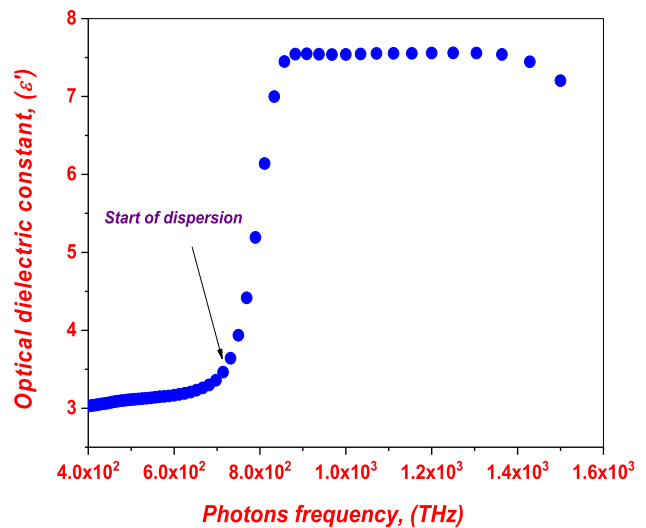
Figure 5a, b illustrates the variation in the values of both  $\epsilon'$  and  $\epsilon''$  with the increase in the frequency of the incident photons. It is obvious that at low frequencies (lower than 8000 THz), each  $\epsilon'$  and  $\epsilon''$  has a constant value, while at high frequencies (higher than 8000 THz), both  $\epsilon'$  and  $\epsilon''$  started to disperse at 8000 THz and then increased to reach their maximum values at 9000 THz, approximately. After that point, 9000 THz,  $\epsilon'$  showed a saturated state while  $\epsilon''$  decreased linearly at a different rate. As an advanced step to understanding the behavior of both  $\epsilon'$  and  $\epsilon''$ , the experimental rate of  $\epsilon''$  has been chosen to fit using the Cole–Cole equation as a novel approximation for studying optical dielectric relaxation

$$\epsilon'' = \frac{(\epsilon_0 - \epsilon_\infty)(\omega\tau_d)}{1 + (\omega\tau_d)^2} \tag{6a}$$

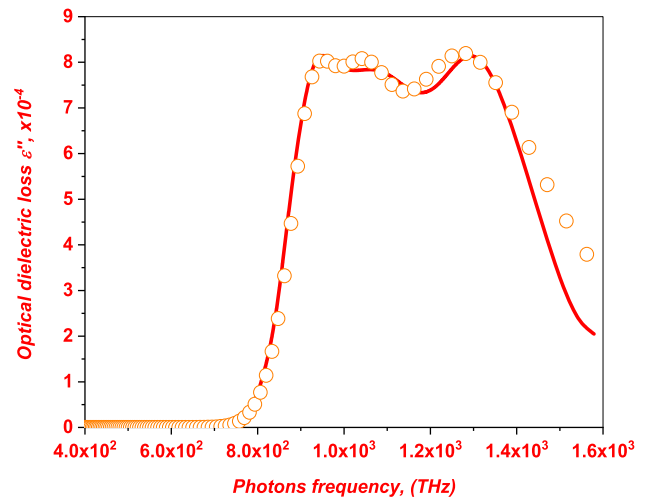
$$\epsilon'' = \frac{(\epsilon_0 - \epsilon_\infty) [(\omega\tau_d)^{1-\zeta} \cos(\frac{\zeta\pi}{2})]}{[1 + (\omega\tau_d)^{1-\zeta} \sin(\frac{\zeta\pi}{2}) + \omega\tau_d^{2(1-\zeta)}]} \tag{6b}$$

(where  $\epsilon''$  is the real dielectric loss,  $\epsilon_0$  is the static dielectric constant,  $\epsilon_\infty$  is the high-frequency dielectric constant,  $\omega$  is the angular frequency,  $\tau_d$  is the dielectric relaxation time, and  $\zeta$  is the Cole–Cole parameter).

The ordinary Cole–Cole formula Eq. 6a, b [16] contains only one term for one relaxation mechanism. Hosam M. Gomaa, the initial author, changed Eq. (6b) to take the form of Eq. 7, which has many terms, each of which denotes a distinct relaxation process (relaxation time) with a separate activation energy. This alteration was based on the simultaneous occurrence of many electronic transitions caused by high-energy electromagnetic waves (UV–Vis light)



(a)



(b)

**Fig. 5** **a** Optical dielectric constant versus the frequency of the photon in THz. **b** Simulated and experimental optical dielectric loss versus the frequency of the photon in THz

$$\begin{aligned} \epsilon'' = & \frac{(\epsilon_0 - \epsilon_\infty) [(\omega\tau_{d1})^{1-\zeta} \cos(\frac{\zeta\pi}{2})]}{[1 + (\omega\tau_{d1})^{1-\zeta} \sin(\frac{\zeta\pi}{2}) + \omega\tau_{d1}^{2(1-\zeta)}]} \\ & + \frac{(\epsilon_0 - \epsilon_\infty) [(\omega\tau_{d2})^{1-\zeta} \cos(\frac{\zeta\pi}{2})]}{[1 + (\omega\tau_{d2})^{1-\zeta} \sin(\frac{\zeta\pi}{2}) + \omega\tau_{d2}^{2(1-\zeta)}]} \\ & + \frac{(\epsilon_0 - \epsilon_\infty) [(\omega\tau_{d3})^{1-\zeta} \cos(\frac{\zeta\pi}{2})]}{[1 + (\omega\tau_{d3})^{1-\zeta} \sin(\frac{\zeta\pi}{2}) + \omega\tau_{d3}^{2(1-\zeta)}]} + \dots \end{aligned} \tag{7}$$

(where  $\tau_{d1}$ ,  $\tau_{d2}$ , and  $\tau_{d3}$  are the relaxation times of different relaxation process)

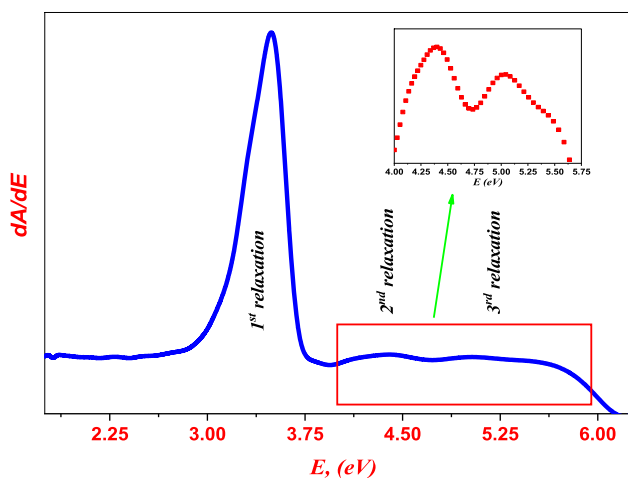


**Fig. 6** Rate of absorption change with energy versus the photon energies

$$\tau_{di} = \tau_{oi} e^{\frac{\Delta E_i}{kT}}, i = 1, 2 \tag{8}$$

(where  $\tau_{di}$  is the dielectric relaxation time corresponding to the activation energy  $\Delta E_i$ ,  $\tau_o$  is the characteristic relaxation time,  $k$  is Boltzmann constant, and  $T$  is the Absolute temperature).

Equation 8 shows that the dielectric relaxation time is a function of both the characteristic relaxation time  $\tau_o$  and the dielectric activation energy  $\Delta E$  which in most cases is close to the value of the activation energy of the DC conduction [18]. Generally, the Cole–Cole formula contains a lot of useful parameters like the high-frequency and low-frequency dielectric constants  $\{\epsilon_o, \epsilon_\infty\}$ , and the parameter  $\{\zeta\}$  which is enclosed between 0 and 1.

Figure 6b is a representative figure that exhibits the experimental and simulated dielectric loss as a function of the frequency of the photons. It is noticed that there is a large consistency between the measured and calculated dielectric loss factors. Such consistency resulted in some parameters that are recorded in Table 2, which shows only one value for the characteristic relaxation time and three values for the Cole–Cole parameter. Such a result can be explained

by imagining multiple relaxation mechanisms. Table 2 also shows that there are three activation energies, which in turn means a distribution of relaxation times for three different charge carriers, (electrons, Plasmon, and metal cation). Where, the observed decrease in the values of the activation energies explains the decrease in the value of optical transmittance in the high-energy region (above 3.5 eV, Fig. 3).

In general, the suggested simulation method reveals about three relaxation processes with different activation energies. To check the validity of this result, the optical absorbance ( $A$ ) has been calculated using Eq. 9, and then,  $dA/dE$  was plotted versus the photon energies as shown in Fig. 5 which shows three maximum limits of the change of  $dA/dE$  versus  $E$ , which refers to three different relaxation processes, which confirm the validity of the previous simulation process. The observed maxima are located at an energy point that has a value that converges with that obtained from the simulation process

$$A = 2 - \log \frac{1}{T} \tag{9}$$

(where  $A$  is the optical absorbance and  $T$  is the optical transmittance).

Pines and Bohm et al. [25, 26] stated that when the charge carrier moves throughout the matter body or on its surface amount of energy should be lost, which is known as surface energy loss, SELF, and volume energy loss, VELF, functions, Eqs. 10 and 11, respectively

$$SELF = \frac{\epsilon''}{(\epsilon' + 1)^2 + \epsilon''^2} \tag{10}$$

$$VELF = \frac{\epsilon''}{\epsilon' + \epsilon''^2} \tag{11}$$

(where  $\epsilon'$  is the real dielectric constant, and  $\epsilon''$  is the dielectric loss).

As shown in Fig. 6, as the frequency increased up to 8000 THz, the values of SELF and VELF remained constant. While, when the frequency exceeds 8000 THz, both SELF and VELF decreased linearly to reach their lowest values at 9000 THz, and then showed no response to the photons

**Table 2** Cole–Cole simulation parameters

	$i=1$	$i=2$	$i=3$
$\Delta E$ (eV)	3.35	4.5	525
$\lambda$ (nm)	370	282	239
Corresponding electronic transition [28–36]	Electronic transitions related to the divalent lead cations $Pb^{2+}$		Electronic transitions related to the non-bridging oxygen atoms
$\xi$ (Cole–Cole parameter)	0.35		
$\tau_o$ (s)	$5 \times 10^{-310}$	$4 \times 10^{-33}$	$3 \times 10^{-34}$

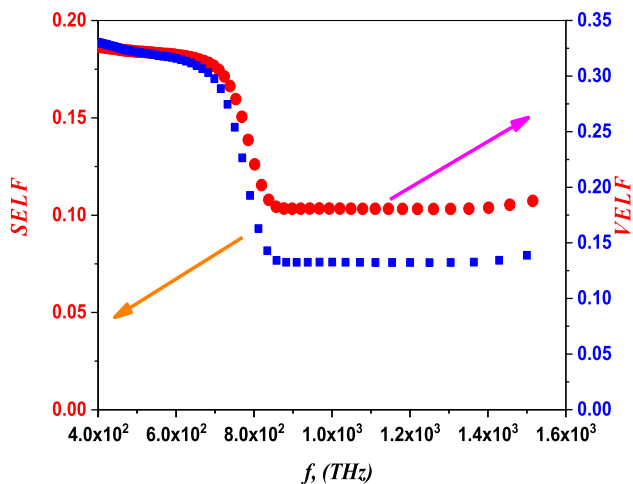


**Fig. 7** SELF and VELF versus the photon frequency

falling. Also, it is noticeable that the VELF values are higher than SELF values, the thing which may be evidence that the probability of light–matter interaction is higher inside the body of the sample than on its surface, which in turn explains the low values of T% (percentage of the optical transmittance). In other words, the optical analysis showed that both the surface and energy loss function (SELF) and the volume energy loss function (VELF) decreased as the photon's frequency increased. The SELF values are found to be lesser than the VELF values, which means that the prepared sample has a high absorption rate and a low reflection rate at all UV–Vis regions. Cole–Cole parameter showed small values (less than unity), confirming the amorphous nature of the prepared sample (Fig. 7).

## 4 Conclusions

One sample of the well-known sodium borate glass has been prepared based on the fast-quenching method. Both XRD and FTIR reveal the amorphous nature of that sample with a glass network composed of three structural units:  $\text{BO}_3$ ,  $\text{BO}_4$ , and  $\text{PbO}_4$ . The optical measurements showed a low transmittance value (less than 50%) with a high absorption rate per unit length. The Cole–Cole approximation has been modified to describe the optical dielectric relaxation process in the optical materials. The parameters resulting from the Cole–Cole simulation process showed how more than one relaxation process, and different charge carriers, contribute to increasing the optical dielectric response. The new modification makes it possible to use the Cole–Cole approximation to determine the hidden absorption peaks in the UV region. These findings should be useful in the field of optical characterization as well

as the research and application area of the optoelectronic field.

**Acknowledgements** The authors extend their appreciation to the Deanship of Scientific Research at King Khalid University for funding this work through the large research group program number: R.G.P.2/434/44.

**Author contributions** Hosam M Gomaa suggested the research idea, performed all analysis and mathematical calculations, and wrote the primary/final manuscript. Saeid M. Elkatlawy reviewed the primary version. H. A. Saudi, H. Y. Zahran, and I. S. Yahia prepared sample, performed the experimental measurements, and reviewed the final version.

**Availability of data and materials** All data will be available when required.

## Declarations

**Conflict of interest** The authors declare that there is no conflict of interest. Author has no relevant financial.

**Ethical approval** This study is not human and/or animal studies (not applicable).

## References

1. M. Bengisu, *J. Mater. Sci.* **51**, 2199 (2016)
2. L. Koudelka, P. Mošner, M. Zeyer, C. Jäger, *J. Non. Cryst. Solids* **326–327**, 72 (2003)
3. M. Abdel-Baki, F. El-Diasty, *Curr. Opin. Solid State Mater. Sci.* **10**, 217 (2006)
4. Y.B. Saddeek, K. Aly, G. Abbady, N. Afify, K.S. Shaaban, A. Dahshan, *J. Non. Cryst. Solids* **454**, 13 (2016)
5. S. Singh, G. Kalia, K. Singh, *J. Mol. Struct.* **1086**, 239 (2015)
6. Y.B. Saddeek, M.S. Gaafar, *Mater. Chem. Phys.* **115**, 280 (2009)
7. A.N. D'Souza, N.S. Prabhu, K. Sharmila, M.I. Sayyed, H.M. Somshekarappa, G. Lakshminarayana, S. Mandal, S.D. Kamath, *J. Non. Cryst. Solids* **542**, 120136 (2020)
8. S. C. Kim, J. R. Choi, and B. K. Jeon, *Sci. Rep.* **6**, (2016).
9. H. A. Saudi, H. M. Gomaa, E. S. H. El-Mosallamy, and S. M. Elkatlawy, *Polym. Polym. Compos.* (2021).
10. H. M. Gomaa, M. I. Sayyed, H. O. Tekin, G. Lakshminarayana, and A. H. EL-Dosokey, *Phys. B Condens. Matter* **567**, 109 (2019).
11. H. M. Gomaa, I. S. Yahia, B. M. A. Makram, A. H. El-Dosokey, and S. M. Elkatlawy, *J. Mater. Sci. Mater. Electron.* (2021).
12. N. Hao, G. Zhang, Z. Yang, G. Qin, H. Jin, S. Gao, *J. Non. Cryst. Solids* **601**, 122042 (2023)
13. S. Li, Y. Lu, Y. Qu, J. Kang, Y. Yue, X. Liang, *J. Non. Cryst. Solids* **556**, 120550 (2021)
14. M. Shapaan, F.M. Ebrahim, *Phys. B Condens. Matter* **405**, 3217 (2010)
15. H. Kchaou, K. Karoui, K. Khirouni, and A. Ben Rhaiem, *J. Alloys Compd.* **728**, 936 (2017).
16. K.S. Cole, R.H. Cole, *J. Chem. Phys.* **9**, 341 (1941)
17. T.D. AbdelAziz, F.M. EzzElDin, H.A. El Batal, A.M. Abdelghany, *Spectrochim. Acta Part A Mol. Biomol. Spectrosc.* **131**, 497 (2014)
18. H.M. Gomaa, *J. Non. Cryst. Solids* **481**, 51 (2018)



19. M. K. El-Mansy, H. M. Gomaa, N. Hendawy, and A. Sabry Morsy, *J. Non. Cryst. Solids* **485**, 42 (2018).
20. H.M. Gomaa, H.A. Saudi, I.S. Yahia, M.A. Ibrahim, H.Y. Zahrán, *Optik (Stuttg)*. **249**, 168267 (2022)
21. N.A. Ghoneim, A.M. Abdelghany, S.M. Abo-Naf, F.A. Moustafa, K.M. ElBadry, *J. Mol. Struct.* **1035**, 209 (2013)
22. M. Salem, T.Z. Abou-elnasr, W.A. El-gammal, A.S. Mahmoud, H.A. Saudi, A.G. Mostafa, *Am. J. Aerosp. Eng.* **5**, 1 (2018)
23. R. Boda, M.D. Shareefuddin, M.N. Chary, R. Sayanna, *Mater. Today Proc.* **3**, 1914 (2016)
24. H.M. Gomaa, I.S. Yahia, *J. Comput. Electron.* **21**, 1396 (2022)
25. H.M. Gomaa, S.M. Elkatlawy, I.S. Yahia, H.A. Saudi, A.M. Abdel-Ghany, *Optik (Stuttg)*. **244**, 167543 (2021)
26. A.S. Hassanien, I. Sharma, *Optik (Stuttg)*. **200**, 163415 (2020)
27. V. Ganesh, I.S. Yahia, S. AlFaify, M. Shkir, *J. Phys. Chem. Solids* **100**, 115 (2017)
28. M.K. El-Mansy, H.M. Gomaa, N. Hendawy, A. Sabry Morsy, *J. Non-Crystalline Solids* **485**(January), 42–46 (2018)
29. N.A. Ghoneim, A.M. Abdelghany, S.M. Abo-Naf, F.A. Moustafa, K.M. Elbadry, *J. Molecular Structure* **1035**(October), 209–217 (2013)
30. M.S. Eluyemi, M.A. Eleruja, A.V. Adedeji, B. Olofinjana, O. Fasakin, O.O. Akinwunmi, O.O. Ilori, A.T. Famojuro, S.A. Ayinde, E.O.B. Ajayi, *Graphene* **05**(03), 143–154 (2016)
31. K.A. Naseer, G. Sathiyapriya, K. Marimuthu, T. Piotrowski, M.S. Alqahtani, E.S. Yousef, *Optik* **251**(December), 168436 (2022)
32. Uran, S., Alhani, A., & Silva, C., *AIP Advances*, **7**(3) (2017).
33. Zhang, T., Zhu, G. Y., Yu, C. H., Xie, Y., Xia, M. Y., Lu, B. Y., Fei, X., & Peng, Q., *Microchimica Acta*, **186**(3). (2019).
34. Manoratne, C. H., Rosa, S. R. D., & Kottegoda, I. R. M., *Material Science Research India*, **14**(1) (2017).
35. AL-Gahouari, T., Sayyad, P., Bodkhe, G., Ingle, N., Mahadik, M., Shirsat, S., & Shirsat, M., *Applied Physics A: Materials Science and Processing*, **127**(3), 1–16 (2021).
36. Marzouk, M. A., ElBatal, H. A., Hamdy, Y. M., & Ezz-Eldin, F. M., *International Journal of Optics* (2019).

**Publisher's Note** Springer Nature remains neutral with regard to jurisdictional claims in published maps and institutional affiliations.

Springer Nature or its licensor (e.g. a society or other partner) holds exclusive rights to this article under a publishing agreement with the author(s) or other rightsholder(s); author self-archiving of the accepted manuscript version of this article is solely governed by the terms of such publishing agreement and applicable law.